Science

RESEARCH ARTICLES

Cite as: Deng *et al*., *Science*
10.1126/science.aed1656 (2026).

Protein-templated synthesis of dinucleotide repeat DNA by an antiphage reverse transcriptase

Pujuan Deng[1,2]†, Hyunbin Lee[1,2]†, Carlo Armijo[1,3]†, Haoqing Wang[4], Alex Gao[1,2]*

[1]Department of Biochemistry, Stanford University, Stanford, CA, USA. [2]Department of Microbiology and Immunology, Stanford University, Stanford, CA, USA. [3]Department of Biology, Stanford University, Stanford, CA, USA. [4]Sarafan ChEM-H, Stanford University, Stanford, CA, USA.

†These authors contributed equally to this work.

*Corresponding author. Email: algao@stanford.edu

Defense-associated reverse transcriptases (DRTs) are widespread bacterial anti-phage systems that use unconventional mechanisms of polynucleotide synthesis. We show that DRT3, which comprises two distinct RTs (Drt3a and Drt3b) and a noncoding RNA (ncRNA), synthesizes alternating poly(GT/AC) double-stranded DNA. Cryo–electron microscopy structures at 2.6 Å resolution reveal a D3-symmetric 6:6:6 complex of Drt3a, Drt3b, and ncRNA. Drt3a produces the poly(GT) strand using a conserved ACACAC template within the ncRNA. Notably, Drt3b synthesizes a complementary, protein-primed poly(AC) strand in the complete absence of a nucleic acid template, using conserved active site residues specific to Drt3b to enforce precise base alternation. These findings expand the functional landscape of nucleic acid polymerases, revealing a protein-templated mechanism for sequence-specific DNA synthesis.

The enzymatic synthesis of nucleic acids is a fundamental process that underlies genome replication, repair, and diverse forms of information processing across all domains of life. Nucleic acid polymerases fall into two broad functional classes: template-directed polymerases, which copy existing nucleic acid sequences (*1*–*5*), and template-independent polymerases. The products of this latter class are typically highly constrained in their complexity, consisting of either long polymers with low sequence complexity, such as homopolymers (*6*, *7*) and near-random 3′-end tracts (*8*, *9*), or short, defined motifs (*10*–*15*). A rare exception is the eukaryotic nucleotidyltransferase RDE-3, which adds alternating poly(UG) tracts onto the 3′ ends of RNA to facilitate RNA interference (*16*, *17*). However, among the vast diversity of uncharacterized proteins, it remains unknown whether distinct modes of nucleotide polymerization exist.

Recently, bacterial defense-associated reverse transcriptases (DRTs) have emerged as a rich source of novel polymerization mechanisms. These enzymes, which are members of a large branch of "unknown group" (UG) RTs (*18*–*20*) and confer resistance to phage infection, display highly divergent activities. For example, AbiK catalyzes protein-primed, terminal deoxynucleotidyl transferase (TdT)-like random nucleotide addition (*21*–*23*), DRT9 synthesizes protein-primed poly(dA) tracts (*24*–*26*), and DRT2 generates long, repetitive cDNA concatemers that reconstitute a novel gene not encoded by the genome (*27*, *28*). Among the diverse UG RTs, DRT3 is unique in its composition, consisting of two reverse transcriptases from distinct clades (*18*)—Drt3a (a class 2 UG RT, also known as UG3) and Drt3b (a class 1 UG RT, also known as UG8)—together with an associated noncoding RNA (*29*). Here, we investigated the function of DRT3 and its mechanism of nucleic acid synthesis.

DRT3 forms a ribonucleoprotein complex that synthesizes alternating dinucleotide DNA

A comprehensive phylogenetic analysis identified diverse DRT3 homologs that are sporadically distributed across at least 20 bacterial phyla (Fig. 1A and data S1 to S6). The topologies of individual Drt3a and Drt3b trees are largely congruent (fig. S1), suggesting co-evolution between these proteins. We cloned two DRT3 systems—one from *Escherichia coli* GF3-3 (EcDRT3) and the previously reported system from *E. coli* ECOR12 (Ec2DRT3) (*29*)—which share 32% amino acid identity (Fig. 1A and data S7). Both systems conferred robust defense against phages T1, T4, and T5 when heterologously expressed in *E. coli* K-12, and defense activity required both RT active sites and the ncRNA (Fig. 1B and fig. S2A), consistent with previous observations (*29*). To characterize putative products synthesized by DRT3, we performed tagmentation sequencing on lysates from cells expressing EcDRT3 or Ec2DRT3, which revealed phage-independent production of double-stranded DNA (dsDNA) consisting of poly(GT/AC) dinucleotide repeats (Fig. 1, C to E, and fig. S2B).

To characterize DRT3 biochemically, we co-expressed the entire EcDRT3 locus in *E. coli* with an internal His_6 tag on Drt3a, which preserves anti-phage activity (fig. S2C). Affinity purification followed by size-exclusion chromatography (SEC) revealed a stable, high molecular weight complex (Fig. 1F). SDS–polyacrylamide gel electrophoresis (PAGE) confirmed this complex consisted of Drt3a and Drt3b at approximately equal stoichiometry, along with a co-purifying nucleic acid band (Fig. 1G and fig. S3A). TBE-Urea PAGE indicated this band was ~130 nt in length and was sensitive

to ribonuclease (RNase) treatment (Fig. 1H and fig. S3B), confirming it was RNA. Small RNA sequencing identified this RNA as the EcDRT3 ncRNA (Fig. 1I, fig. S2D, and data S8). Together, these results indicate that EcDRT3 forms a ribonucleoprotein (RNP) complex consisting of Drt3a, Drt3b, and the ncRNA.

Incubation of the purified EcDRT3 RNP complex with deoxynucleotide triphosphates (dNTPs) in vitro resulted in a substantial increase in the apparent molecular weight of the Drt3b subunit, whereas Drt3a remained unchanged (Fig. 1J). This shift was abolished in complexes harboring a Drt3b active site mutation (D291A/D292A; '3b YVAA') but retained with a Drt3a mutation (D197A/D198A; '3a YVAA') and with apo Drt3b alone (Fig. 1J and fig. S2E), indicating that Drt3b synthesizes DNA that remains covalently attached to the protein.

Agarose gel electrophoresis of the EcDRT3 in vitro reaction (Fig. 1K) revealed a DNA product of heterogeneous size extending up to several kilobases (Fig. 1L). The product was partially resistant to both S1 nuclease [which degrades single-stranded DNA (ssDNA)] and duplex deoxyribonuclease (DNase), indicating that EcDRT3 produces both ssDNA and dsDNA. The S1-resistant fraction was more pronounced after proteinase K digestion, consistent with some of the ssDNA product being covalently attached to Drt3b. Furthermore, the overall product was not sensitive to RNase treatment and included species smaller than the ncRNA (fig. S2F), suggesting the absence of an ncRNA-DNA covalent linkage.

In vitro assays of active site mutants revealed distinct roles for each RT. The Drt3a mutant (retaining only Drt3b activity) produced S1-sensitive ssDNA that was detectable only after proteinase K treatment (Fig. 1L), consistent with covalent attachment to Drt3b. The Drt3b mutant (retaining only Drt3a activity) also generated S1-sensitive ssDNA, but in this case the product was equally visible with or without proteinase K (Fig. 1L). Mixing the two ssDNA products resulted in an increased band intensity (Fig. 1M) and a shift in gel staining hue (fig. S2G), indicative of annealing of complementary strands to form dsDNA. Corroborating this, dsDNA tagmentation sequencing of the wild-type in vitro reaction product yielded both poly(GT) and poly(AC) reads (Fig. 1N), confirming that DRT3 synthesizes both strands of the dinucleotide repeat.

Cryo-EM structures of the EcDRT3 complex

To understand how Drt3a, Drt3b, and the ncRNA assemble and coordinate complementary strand synthesis, we determined two cryo–electron microscopy (cryo-EM) structures of the EcDRT3 complex—a −dNTP resting state and a +dNTP elongating state—each at 2.6 Å resolution (Fig. 2A–B, fig. S4, S5, and S6A–B, table S1). Both structures reveal a D3-symmetric assembly containing six copies each of Drt3a, Drt3b, and the ncRNA (Fig. 2, A and B, and fig. S6, A and B). The fundamental unit is a 1:1:1 Drt3a–Drt3b–ncRNA protomer; three protomers assemble into a trimer, and two trimers dimerize tail-to-tail to form the final hexamer (Fig. 2B). The two states are globally similar, with a root mean square deviation (RMSD) of ~0.302 Å between the core Drt3b hexamers (fig. S6C). Intra-trimer stability is driven by extensive Drt3a–Drt3b and Drt3b–Drt3b contacts (Fig. 2B–F), including a cyclical salt-bridge network between Glu389 and Arg390 of the three Drt3b subunits (Fig. 2E). The inter-trimer interface is mediated by opposing Drt3b RT domains and stabilized by interactions between at least seven residues (Fig. 2, G and H), burying ~1,768 $Å^2$ of surface area. Furthermore, a DNA product duplex is positioned around the exterior of the complex (Fig. 2I). The dimer-of-trimers arrangement of Drt3b subunits resembles that of AbiK (*23*) but differs from the trimer-of-dimers configuration of DRT9 (*24*–*26*) (fig. S6D).

Drt3a synthesizes poly(GT) ssDNA templated by ncRNA

To investigate the activity of the Drt3a subunit, we assayed DNA synthesis in vitro without proteinase K treatment using various dNTP combinations with wild-type EcDRT3 (Fig. 3A), the Drt3b YVAA mutant complex (fig. S7A), or a Drt3a–ncRNA subcomplex lacking Drt3b (fig. S7B). For all three, an ssDNA product was detected only when both dGTP and dTTP were present in the reaction, while deoxyadenosine triphosphate (dATP) and deoxycytidine triphosphate (dCTP) were dispensable. Sequencing of the product synthesized by EcDRT3 with all four dNTPs revealed that it consisted of poly(GT) dinucleotide repeats (Fig. 3B).

Drt3a adopts a canonical right-hand (fingers–palm–thumb) fold, and structural comparisons show close similarity to other RTs, including class 2 UG RTs (e.g., DRT2, DRT9), a group II intron RT (*30*), and telomerase (*31*) (Fig. 3C and fig. S8, A and B). The ncRNA, which contains four stem-loops (SL1-4), wraps around the Drt3a thumb domain (Fig. 3C), positioning its conserved $A^{108}CACAC^{113}$ motif (*20*) in the active site to template poly(GT) synthesis (Fig. 3C and figs. S2D and S8C), with A108 as the templating base. The nascent cDNA is clearly resolved as a product–template duplex. The resting state contains a 5 nt product (TGTGT) in the active site, whereas all 6 nucleotides were resolved in the elongating state (fig. S8A). In both structures, the product strand extends to the final base of the template, consistent with a post-synthesis state prior to strand separation.

The product–template duplex is anchored predominantly through non-sequence-specific contacts with the sugar–phosphate backbone. In particular, Drt3a forms five hydrogen bonds with A108 and the 3′ end of the cDNA product (dT15 and dG16) (Fig. 3D), positioning these bases for polymerization (fig. S9A). On the cDNA strand, Tyr343 and Tyr195 (from the YVDD motif) contact the dT15 (*n*–2) phosphate and base, respectively, while Lys289 coordinates the dG16 (*n*–1) phosphate. On the template side, A108 is held in place by a hydrogen bond between its 2′-OH and the backbone carbonyl of Gly164 (Fig. 3D). Gly164 is a part of the canonical RT-4 motif (GxxxGxxxS) (*32*), suggesting a conserved

strategy for backbone-mediated positioning of the templating base (fig. S9A).

The single-stranded RNA template region (A108–C113) is sandwiched between two adjacent stem-loops, SL1 and SL4, both of which are anchored to Drt3a via π–π interactions: Tyr419 stacks with the G98–C107 base pair of SL4 (Fig. 3E), whereas Phe402 stabilizes the U19–A116 base pair of SL1 (Fig. 3F). Additionally, Arg335 stabilizes C113 through a cation–π interaction (Fig. 3G). The downstream U114–A115 region appears flexible, with clear backbone density only in the elongating state. This flexibility facilitates a conformational change that reduces the C113–A116 inter-phosphate distance from 15.4 Å to 10.3 Å in the resting state (Fig. 3, C to H, and fig. S8A), likely shifting C109 by one nucleotide into the templating position. These observations indicate that A108 and C109 serve as the templating bases, while A110–C113 stabilize the nascent product strand (Fig. 3H and fig. S9B). Consistent with this model, both A108G (GCACAC) and C109T (ATACAC) mutants failed to produce DNA products both in vitro (Fig. 3I) and in *E. coli* (fig. S9C) and abolished defense (Fig. 3J).

A unique β-hairpin extension within the Drt3a thumb domain (residues 323–338) is positioned immediately after the 3′ base of the template motif (C113) (Fig. 3C). The presence of this β-hairpin is conserved across DRT3 homologs and may function as a "zipper head" to dissociate the product–template duplex following each cycle of dinucleotide addition, a mechanism analogous to the thumb loop (TH) of telomerase (*33*) (fig. S9D). In contrast, in DRT2, the ncRNA itself appears to perform this role, guiding the cDNA to thread back into the ncRNA scaffold (fig. S9D).

Drt3b synthesizes poly(AC) ssDNA de novo without a nucleic acid template

To investigate Drt3b-mediated ssDNA synthesis, we performed in vitro assays using a catalytically inactive Drt3a (3a YVAA) complex or apo Drt3b. In both cases, ssDNA was produced only when both dATP and dCTP were present (Fig. 4A and fig. S10A). Sequencing of the 3a YVAA product synthesized in the presence of all four dNTPs confirmed that it consisted of alternating poly(AC) (Fig. 4B). Incubating the wild-type EcDRT3 complex with dGTP+dTTP or dATP+dCTP suggested that the poly(AC) ssDNA is shorter than the corresponding poly(GT) synthesized by Drt3a (fig. S10B).

In both elongating and resting complexes, the poly(AC) ssDNA product occupies the Drt3b active site in the complete absence of a nucleic acid template (Fig. 4C). While adopting a canonical RT fold (fig. S10, C to G), Drt3b possesses unique features that preclude template binding (Fig. 4, C and D). The template-binding channel is occluded by the Drt3b C terminus (residues 645–650) and an extended, Drt3b-specific internal loop (residues 112–169) that sandwiches the C-terminal segment. Moreover, the Drt3b N terminus, particularly the conserved Glu26, occupies the space where a template strand would normally reside (Fig. 4D).

The absence of a template is striking given the poly(AC) product sequence, which implies a highly specific, regulated incorporation mechanism. The nascent cDNA strand exhibits an unusual backbone kink that compresses three bases (dC15–dA16–dC17) into a space normally occupied by two (Fig. 4E). This distorted geometry enables an extensive network of protein–DNA base interactions, effectively acting as a protein-based template to replace nucleic acid (Fig. 4, F and G). This contrasts with templated polymerases, which lack direct interaction between cDNA bases and protein residues beyond the conserved YxDD motif tyrosine.

Two conserved active site residues, Glu26 and Arg253, enforce the sequential incorporation of dA and dC through base-specific contacts (Fig. 4, F and G). The Glu26 side chain projects into the nucleotide-binding pocket and mimics a templating nucleobase, forming two hydrogen bonds with the N^6 amine of dA18 to discriminate dATP from deoxyguanosine triphosphate (dGTP) and deoxythymidine triphosphate (dTTP) (Fig. 4F and fig. S11A). Although dCTP also possesses an exocyclic amine (N^4), its smaller pyrimidine ring likely prevents productive hydrogen bonding with Glu26 and also attenuates the stabilizing cation-π interaction with Arg253 (Fig. 4G and fig. S11A). Additionally, the Arg253 guanidinium group and Glu26 side chain form three hydrogen bonds with the Watson-Crick edge of the preceding dC17, distinguishing dC from dT (Fig. 4F and fig. S11B). Steric exclusion of bulky purines (dA, dG) further restricts this position to dC (fig. S11B). These specific interactions distinguish Drt3b from other template-independent DRTs (AbiK, AbiP2, and AbiA), which lack these key residues and consequently generate non-specific cDNA (fig. S11C) (*23*, *34*).

To investigate the templating role of Glu26, we purified mutants perturbing (E26Q) or abolishing (E26A) its hydrogen-bonding capacity (fig. S11A). The E26A variant produced severely truncated cDNA, establishing that Glu26-mediated hydrogen bonding is essential for efficient polymerization (Fig. 4H). Both mutants synthesized cDNA with dATP and dCTP; however, adding dGTP to the reaction substantially reduced efficiency and drove dG misincorporation at dA sites, while preserving fidelity at dC sites (Fig. 4, H to J, and fig. S11D). The addition of dTTP did not alter these trends (Fig. 4, H to J). Consistently, both mutants abolished anti-phage defense and poly(GT/AC) dsDNA synthesis in *E. coli* (fig. S11, E and F). Thus, Glu26 acts as a critical gatekeeper for dA selection, whereas dC incorporation depends on distinct templating residues. The strong purine preference at the incoming dA site likely arises from a cation-π interaction with Arg253 (Fig. 4G), while a steric clash between Gly248 and the exocyclic amine (N^2) of dG maintains the residual preference for dA over dG in both Glu26 mutants (~80% vs ~20%; fig. S11A). Attempts to capture the dC-adding state using ddATP and dCTP yielded a cryo-EM map identical to the dA-adding state (fig. S12).

Beyond dA18 and dC17, the preceding four bases (dC13 to dA16) also engage in direct contacts with Drt3b residues—

including base-specific (dC13–Arg408), purine-specific (dA16–Thr335/Thr338), pyrimidine-specific (dC15–Arg168/Tyr289), and non-specific (dA14–Tyr170) interactions—that further stabilize the kinked ssDNA. In contrast, predicted structures of RDE-3 complexed with poly(UG) RNA (protein–RNA ipTM 0.94) lack these stabilizing contacts (Fig. 4, E to G, and fig. S10G). Altogether, this extensive network of base-specific and conformation-stabilizing interactions spanning dC13 to dA18 provides the protein template that dictates precise alternating poly(AC) synthesis.

Finally, we observed weak additional density near the hydroxyl group of the C-terminal Tyr650, suggesting a covalently attached phosphate from a protein–DNA adduct (fig. S13A). The hydroxyl-bearing side chain at this position (Tyr, or occasionally Ser) is conserved across DRT3 homologs, supporting its role as the nucleophile that initiates DNA synthesis (fig. S13B). Corroborating this model, a Drt3b-Y650F mutant did not exhibit a dNTP-dependent molecular weight shift on SDS-PAGE (fig. S13C), indicating loss of covalent adduct formation. The Y650F mutation also abolished phage defense (fig. S13D) and in vivo dsDNA accumulation (fig. S13E), demonstrating that Tyr650-mediated priming is essential for DRT3 function. Tyrosine priming is consistent with several other DRT systems, including AbiK (*22*, *23*), Abi-P2 (*23*), AbiA (*34*), and DRT9 (*24–26*).

Phage T1 protein ST61 is required for EcDRT3-mediated defense

To understand the requirements for DRT3 defense, we isolated five distinct phage T1 escape mutants via adaptive evolution (Fig. 5, A and B). These mutants exhibited robust escape from EcDRT3 and partial escape from Ec2DRT3 (fig. S14A). All five harbored inactivating mutations within a single uncharacterized gene, ST61 (Fig. 5B). Co-expressing ST61 and EcDRT3 was constitutively toxic to *E. coli*, and this toxicity was abolished when Drt3a, Drt3b, or the ncRNA was disrupted (Fig. 5C). ST61 has a predicted SH3 domain-like fold and is encoded within a four-gene neighborhood conserved across the *Tunavirinae* subfamily of phages (fig. S14B). Sequencing of DRT3-expressing cells infected with escape phages showed a modest reduction in poly(GT) and poly(AC) reads compared to wild-type T1 infection (fig. S14C). Together, these findings identify ST61 as a phage-encoded trigger required to activate DRT3-mediated defense.

Discussion

Our study reveals the DRT3 system as a coordinated bacterial defense complex that synthesizes alternating dinucleotide dsDNA using two mechanistically distinct RTs (Fig. 5D). Drt3a functions as a telomerase-like RNA-templated polymerase, generating poly(GT) ssDNA from the conserved ACACAC motif within the ncRNA. Conversely, Drt3b produces the complementary poly(AC) strand without any nucleic acid template. For Drt3b, precise base alternation is enforced by conserved active site residues, which form base-specific hydrogen bonds that replace canonical Watson-Crick base pairing. While the activities of the individual RTs supports the emerging theme that class 1 UGs synthesize non-templated polymers (*23*, *34–38*) and class 2 UGs generate RNA-templated repeats (*24–28*, *39*), their coordinated synthesis of complementary strands to form dsDNA is unique among DRT systems.

Our cryo-EM structures provide insights into the kinetics of DNA synthesis by Drt3a and Drt3b. For Drt3a, the elongating product is fully extended across the ACACAC template, suggesting that the subsequent strand separation is the rate-determining step of the synthesis cycle, analogous to the mechanism of telomerase (*33*). Similarly, the Drt3b product terminates in a 3′ dA (Fig. 4E and fig. S10F), with no detected structural classes ending in dC, suggesting that the dC-adding state is transient and that product translocation following dA addition is rate-limiting.

In contrast to Drt3a, the Drt3b active site directly encodes the alternating poly(AC) product. Specifically, Glu26 serves as the primary template for dA selection, whereas dC selection likely involves distinct or additional residues. Based on the proximity of Arg253 to the nascent dNTP-binding site and its observed interaction with the preceding dC17, we hypothesize that a rotational shift of the Arg253 side chain, induced by the translocation of dA, disrupts the purine-specific cation-π interaction and facilitates the formation of specific hydrogen bonds with an incoming dCTP, effectively serving as a secondary template during the dC-addition cycle. In this state, the cDNA might adopt a conventional kink-less conformation with an empty Thr335 pocket to maintain the register of the poly(AC) interactions with the protein side chains after translocation. Beyond the immediate insertion site, all six of the final bases (up to and including the 3′ terminal dA) form close contacts with amino acid side chains, including three base-specific and two purine/pyrimidine-specific contacts. This structurally encoded recognition suggests Drt3b cannot be easily reprogrammed for alternative sequence specificities without loss of synthesis efficiency.

This protein-templated mechanism for generating a long, sequence-specific nucleic acid is highly atypical among known polymerases. While some prokaryotic polymerases can generate repetitive dsDNA in vitro (*40–42*), this process remains template-dependent: The polymerase first synthesizes random short primers, and only those that are self-complementary are selectively amplified to yield the alternating repeat (*43*). Limited forms of protein-templated base incorporation also exist, but they typically produce only extremely short products—for example, the CCA motif added to tRNAs by the CCA-adding enzyme (*11–13*), or a single cytosine templated by the DNA translesion polymerase Rev1 (*10*). Functionally, Drt3b most closely resembles the nucleotidyltransferase RDE-3, which adds alternating poly(UG) tracts to RNA 3′ ends (*16*, *17*). However, Drt3b is distinguished by its utilization of an RT fold and its production of DNA; furthermore, AlphaFold 3 models of RDE-3 suggest that Drt3b is distinct in its

extensive sequence-specific stabilization of the nascent product, with protein residues substituting for the structural role of a nucleic acid template.

The alternating poly(GT/AC) product sequence appears to be universal across DRT3 homologs, as indicated by the conservation of the $(AC)_3$ RNA template motif and Drt3b templating residues. The evolutionary investment in two specialized polymerases dedicated to manufacturing a conserved pair of perfectly complementary strands suggests that the repetitive, double-stranded nature of the product is critical for its anti-phage function. Consistently, mutations in either RT abolished defense despite continued production of the complementary ssDNA strand by the other RT in vitro, indicating that both strands of the product are essential. Although the function of the product remains unknown, its repetitive poly(GT/AC) sequence might enable gapped, protein-linked duplexes to assemble into a higher-order network through annealing between multiple strands. Alternatively, or additionally, these repetitive tracts are also prone to adopting non-B-form conformations, such as slipped-strand structures (*44*) or, less likely, Z-DNA (*45*). Such complex structural assemblies might function as "molecular sponges" that titrate essential phage-derived DNA binding proteins, as proposed for DRT9 (*24*, *25*).

The activity of Drt3b contrasts with that of other class 1 UG RTs such as AbiK (*21*), which synthesizes random DNA (*22*) despite sharing a similar overall structure and tyrosine priming mechanism (*23*). The residue-level adaptations specific to Drt3b that enforce dinucleotide periodicity underscore the versatility of the UG RT family. Altogether, the DRT3 system employs an unexpected mechanism of biological information transfer, expanding the remarkable repertoire of nucleic acid–based strategies in antiphage defense.

REFERENCES AND NOTES

1. I. R. Lehman, M. J. Bessman, E. S. Simms, A. Kornberg, Enzymatic synthesis of deoxyribonucleic acid. I. Preparation of substrates and partial purification of an enzyme from *Escherichia coli*. *J. Biol. Chem.* **233**, 163–170 (1958). doi:10.1016/S0021-9258(19)68048-8 Medline
2. S. B. Weiss, Enzymatic incorporation of ribonucleoside triphosphates into the interpolynucleotide linkages of ribonucleic acid. *Proc. Natl. Acad. Sci. U.S.A.* **46**, 1020–1030 (1960). doi:10.1073/pnas.46.8.1020 Medline
3. D. Baltimore, R. M. Franklin, A new ribonucleic acid polymerase appearing after Mengovirus infection of L-cells. *J. Biol. Chem.* **238**, 3395–3400 (1963). doi:10.1016/S0021-9258(18)48679-6 Medline
4. D. Baltimore, RNA-dependent DNA polymerase in virions of RNA tumour viruses. *Nature* **226**, 1209–1211 (1970). doi:10.1038/2261209a0 Medline
5. H. M. Temin, S. Mizutani, RNA-dependent DNA polymerase in virions of Rous sarcoma virus. *Nature* **226**, 1211–1213 (1970). doi:10.1038/2261211a0 Medline
6. M. Edmonds, R. Abrams, Polynucleotide biosynthesis: Formation of a sequence of adenylate units from adenosine triphosphate by an enzyme from thymus nuclei. *J. Biol. Chem.* **235**, 1142–1149 (1960). doi:10.1016/S0021-9258(18)69494-3 Medline
7. R. Aphasizhev, S. Sbicego, M. Peris, S.-H. Jang, I. Aphasizheva, A. M. Simpson, A. Rivlin, L. Simpson, Trypanosome mitochondrial 3′ terminal uridylyl transferase (TUTase): The key enzyme in U-insertion/deletion RNA editing. *Cell* **108**, 637–648 (2002). doi:10.1016/S0092-8674(02)00647-5 Medline
8. F. J. Bollum, Calf thymus polymerase. *J. Biol. Chem.* **235**, 2399–2403 (1960). doi:10.1016/S0021-9258(18)64634-4 Medline
9. F. W. Alt, D. Baltimore, Joining of immunoglobulin heavy chain gene segments: Implications from a chromosome with evidence of three D-JH fusions. *Proc. Natl. Acad. Sci. U.S.A.* **79**, 4118–4122 (1982). doi:10.1073/pnas.79.13.4118 Medline
10. D. T. Nair, R. E. Johnson, L. Prakash, S. Prakash, A. K. Aggarwal, Rev1 employs a novel mechanism of DNA synthesis using a protein template. *Science* **309**, 2219–2222 (2005). doi:10.1126/science.1116336 Medline
11. J. Preiss, M. Dieckmann, P. Berg, The enzymic synthesis of amino acyl derivatives of ribonucleic acid. IV. The formation of the 3′-hydroxyl terminal trinucleotide sequence of amino acid-acceptor ribonucleic acid. *J. Biol. Chem.* **236**, 1748–1757 (1961). doi:10.1016/S0021-9258(19)63296-5 Medline
12. J. J. Furth, J. Hurwitz, R. Krug, M. Alexander, The incorporation of adenylic and cytidylic acids into ribonucleic acid. *J. Biol. Chem.* **236**, 3317–3322 (1961). doi:10.1016/S0021-9258(18)94017-2 Medline
13. Y. Xiong, T. A. Steitz, Mechanism of transfer RNA maturation by CCA-adding enzyme without using an oligonucleotide template. *Nature* **430**, 640–645 (2004). doi:10.1038/nature02711 Medline
14. L. Sun, J. Wu, F. Du, X. Chen, Z. J. Chen, Cyclic GMP-AMP synthase is a cytosolic DNA sensor that activates the type I interferon pathway. *Science* **339**, 786–791 (2013). doi:10.1126/science.1232458 Medline
15. A. T. Whiteley, J. B. Eaglesham, C. C. de Oliveira Mann, B. R. Morehouse, B. Lowey, E. A. Nieminen, O. Danilchanka, D. S. King, A. S. Y. Lee, J. J. Mekalanos, P. J. Kranzusch, Bacterial cGAS-like enzymes synthesize diverse nucleotide signals. *Nature* **567**, 194–199 (2019). doi:10.1038/s41586-019-0953-5 Medline
16. M. A. Preston, D. F. Porter, F. Chen, N. Buter, C. P. Lapointe, S. Keles, J. Kimble, M. Wickens, Unbiased screen of RNA tailing activities reveals a poly(UG) polymerase. *Nat. Methods* **16**, 437–445 (2019). doi:10.1038/s41592-019-0370-6 Medline
17. A. Shukla, J. Yan, D. J. Pagano, A. E. Dodson, Y. Fei, J. Gorham, J. G. Seidman, M. Wickens, S. Kennedy, poly(UG)-tailed RNAs in genome protection and epigenetic inheritance. *Nature* **582**, 283–288 (2020). doi:10.1038/s41586-020-2323-8 Medline
18. K. K. Kojima, M. Kanehisa, Systematic survey for novel types of prokaryotic retroelements based on gene neighborhood and protein architecture. *Mol. Biol. Evol.* **25**, 1395–1404 (2008). doi:10.1093/molbev/msn081 Medline
19. D. M. Simon, S. Zimmerly, A diversity of uncharacterized reverse transcriptases in bacteria. *Nucleic Acids Res.* **36**, 7219–7229 (2008). doi:10.1093/nar/gkn867 Medline
20. M. R. Mestre, L. A. Gao, S. A. Shah, A. López-Beltrán, A. González-Delgado, F. Martínez-Abarca, J. Iranzo, M. Redrejo-Rodríguez, F. Zhang, N. Toro, UG/Abi: A highly diverse family of prokaryotic reverse transcriptases associated with defense functions. *Nucleic Acids Res.* **50**, 6084–6101 (2022). doi:10.1093/nar/gkac467 Medline
21. E. Emond, B. J. Holler, I. Boucher, P. A. Vandenbergh, E. R. Vedamuthu, J. K. Kondo, S. Moineau, Phenotypic and genetic characterization of the bacteriophage abortive infection mechanism AbiK from Lactococcus lactis. *Appl. Environ. Microbiol.* **63**, 1274–1283 (1997). doi:10.1128/aem.63.4.1274-1283.1997 Medline
22. C. Wang, M. Villion, C. Semper, C. Coros, S. Moineau, S. Zimmerly, A reverse transcriptase-related protein mediates phage resistance and polymerizes untemplated DNA in vitro. *Nucleic Acids Res.* **39**, 7620–7629 (2011). doi:10.1093/nar/gkr397 Medline
23. M. Figiel, M. Gapińska, M. Czarnocki-Cieciura, W. Zajko, M. Sroka, K. Skowronek, M. Nowotny, Mechanism of protein-primed template-independent DNA synthesis by Abi polymerases. *Nucleic Acids Res.* **50**, 10026–10040 (2022). doi:10.1093/nar/gkac772 Medline
24. X.-Y. Song, Y. Xia, J.-T. Zhang, Y.-J. Liu, H. Qi, X.-Y. Wei, H. Hu, Y. Xia, X. Liu, Y.-F. Ma, N. Jia, Bacterial reverse transcriptase synthesizes long poly(A)-rich cDNA for antiphage defense. *Science* **388**, eads4639 (2025). doi:10.1126/science.ads4639 Medline
25. S. Tang, R. Žedaveinytė, N. Burman, S. Pandey, J. L. Ramirez, L. M. Kulber, T. Wiegand, R. A. Wilkinson, Y. Ma, D. J. Zhang, G. D. Lampe, M. Berisa, M.

Jovanovic, B. Wiedenheft, S. H. Sternberg, Protein-primed homopolymer synthesis by an antiviral reverse transcriptase. *Nature* **643**, 1352–1362 (2025). doi:10.1038/s41586-025-09179-5 Medline
26. J. Han, B. Liu, J. Tang, S. Zhang, X. Wang, X. Li, Q. Zhang, Z. Liu, W. Wang, Y. Liu, R. Zhou, H. Yin, Y. Wei, Z. Li, M. Zhang, Z. Deng, H. Zhang, Non-coding RNA mediates the defense-associated reverse transcriptase (DRT) anti-phage oligomerization transition. *EMBO J.* **44**, 5429–5442 (2025). doi:10.1038/s44318-025-00544-8 Medline
27. M. E. Wilkinson, D. Li, A. Gao, R. K. Macrae, F. Zhang, Phage-triggered reverse transcription assembles a toxic repetitive gene from a noncoding RNA. *Science* **386**, eadq3977 (2024). doi:10.1126/science.adq3977 Medline
28. S. Tang, V. Conte, D. J. Zhang, R. Žedaveinytė, G. D. Lampe, T. Wiegand, L. C. Tang, M. Wang, M. W. G. Walker, J. T. George, L. E. Berchowitz, M. Jovanovic, S. H. Sternberg, De novo gene synthesis by an antiviral reverse transcriptase. *Science* **386**, eadq0876 (2024). doi:10.1126/science.adq0876 Medline
29. L. Gao, H. Altae-Tran, F. Böhning, K. S. Makarova, M. Segel, J. L. Schmid-Burgk, J. Koob, Y. I. Wolf, E. V. Koonin, F. Zhang, Diverse enzymatic activities mediate antiviral immunity in prokaryotes. *Science* **369**, 1077–1084 (2020). doi:10.1126/science.aba0372 Medline
30. J. L. Stamos, A. M. Lentzsch, A. M. Lambowitz, Structure of a Thermostable Group II Intron Reverse Transcriptase with Template-Primer and Its Functional and Evolutionary Implications. *Mol. Cell* **68**, 926–939.e4 (2017). doi:10.1016/j.molcel.2017.10.024 Medline
31. Y. He, H. Song, H. Chan, B. Liu, Y. Wang, L. Sušac, Z. H. Zhou, J. Feigon, Structure of Tetrahymena telomerase-bound CST with polymerase α-primase. *Nature* **608**, 813–818 (2022). doi:10.1038/s41586-022-04931-7 Medline
32. Y. Xiong, T. H. Eickbush, Origin and evolution of retroelements based upon their reverse transcriptase sequences. *EMBO J.* **9**, 3353–3362 (1990). doi:10.1002/j.1460-2075.1990.tb07536.x Medline
33. Y. He, Y. Wang, B. Liu, C. Helmling, L. Sušac, R. Cheng, Z. H. Zhou, J. Feigon, Structures of telomerase at several steps of telomere repeat synthesis. *Nature* **593**, 454–459 (2021). doi:10.1038/s41586-021-03529-9 Medline
34. M. Gapińska, W. Zajko, K. Skowronek, M. Figiel, P. S. Krawczyk, A. A. Egorov, A. Dziembowski, M. J. O. Johansson, M. Nowotny, Structure-functional characterization of Lactococcus AbiA phage defense system. *Nucleic Acids Res.* **52**, 4723–4738 (2024). doi:10.1093/nar/gkae230 Medline
35. Y. Wang, H. Wu, J. Li, Q. An, Z. Tian, Z. Deng, Anti-phage defense mechanism involving phage-encoded DNA binding protein and bacterial reverse transcriptase DRT4. *Nat. Commun.* **17**, 289 (2025). doi:10.1038/s41467-025-66997-x Medline
36. Y. Wang, H. Wu, J. Li, Z. Tian, Z. Deng, Cryo-EM structure of the bacterial anti-phage defense system DRT6. *Biochem. Biophys. Res. Commun.* **791**, 152955 (2025). doi:10.1016/j.bbrc.2025.152955 Medline
37. M. Figiel, V. K. Viswanath, M. Czarnocki-Cieciura, M. Šoltysová, J. Rybakowska, A. A. Egorov, V. Hauryliuk, M. J. O. Johansson, M. Nowotny, Structures and enzymatic mechanisms of DRT7/UG10 antiphage reverse transcriptases. bioRxiv 2026.02.16.706125 [Preprint] (2026); https://doi.org/10.64898/2026.02.16.706125.
38. S. Kim, H. Xu, G. Mohr, J. Yao, Y. J. Zhang, G. Cui, A. M. Lambowitz, A bacterial PrimPol-reverse transcriptase hybrid protein has a proofreading exonuclease activity that can be transferred to other reverse transcriptases. bioRxiv 2025.09.07.674619 [Preprint] (2025); https://doi.org/10.1101/2025.09.07.674619.
39. S. Tang, J. L. Ramirez, M. R. Mestre, D. J. Zhang, M. Wang, T. Wiegand, Y. Ma, M. Jovanovic, R. Pinilla-Redondo, S. H. Sternberg, Antiviral reverse transcriptases reveal the evolutionary origin of telomerase. bioRxiv 2025.10.16.682844 [Preprint] (2025); https://doi.org/10.1101/2025.10.16.682844.
40. H. K. Schachman, J. Adler, C. M. Radding, I. R. Lehman, A. Kornberg, Enzymatic synthesis of deoxyribonucleic acid. VII. Synthesis of a polymer of deoxyadenylate and deoxythymidylate. *J. Biol. Chem.* **235**, 3242–3249 (1960). doi:10.1016/S0021-9258(20)81345-3 Medline
41. N. Ogata, T. Miura, Genetic information 'created' by archaebacterial DNA polymerase. *Biochem. J.* **324**, 667–671 (1997). doi:10.1042/bj3240667 Medline
42. K. Hanaki, T. Odawara, T. Muramatsu, Y. Kuchino, M. Masuda, K. Yamamoto, C. Nozaki, K. Mizuno, H. Yoshikura, Primer/template-independent synthesis of poly d(A-T) by Taq polymerase. *Biochem. Biophys. Res. Commun.* **238**, 113–118 (1997). doi:10.1006/bbrc.1997.7197 Medline
43. N. V. Zyrina, V. N. Antipova, L. A. Zheleznaya, *Ab initio*synthesis by DNA polymerases. *FEMS Microbiol. Lett.* **351**, 1–6 (2014). doi:10.1111/1574-6968.12326
44. G. Levinson, G. A. Gutman, Slipped-strand mispairing: A major mechanism for DNA sequence evolution. *Mol. Biol. Evol.* **4**, 203–221 (1987). Medline
45. S. Roschdi, T. Kume, R. J. Petersen, A. McCann, C. A. Escobar, A. Richard, S. E. Butcher, Sequence and ionic requirements of pUG fold quadruplexes. bioRxiv 2025.10.28.685102 [Preprint] (2025); https://doi.org/10.1101/2025.10.28.685102.
46. A. M. Burroughs, D. Zhang, D. E. Schäffer, L. M. Iyer, L. Aravind, Comparative genomic analyses reveal a vast, novel network of nucleotide-centric systems in biological conflicts, immunity and signaling. *Nucleic Acids Res.* **43**, 10633–10654 (2015). doi:10.1093/nar/gkv1267 Medline
47. S. F. Altschul, T. L. Madden, A. A. Schäffer, J. Zhang, Z. Zhang, W. Miller, D. J. Lipman, Gapped BLAST and PSI-BLAST: A new generation of protein database search programs. *Nucleic Acids Res.* **25**, 3389–3402 (1997). doi:10.1093/nar/25.17.3389 Medline
48. M. Steinegger, J. Söding, MMseqs2 enables sensitive protein sequence searching for the analysis of massive data sets. *Nat. Biotechnol.* **35**, 1026–1028 (2017). doi:10.1038/nbt.3988 Medline
49. K. Katoh, D. M. Standley, MAFFT multiple sequence alignment software version 7: Improvements in performance and usability. *Mol. Biol. Evol.* **30**, 772–780 (2013). doi:10.1093/molbev/mst010 Medline
50. S. Capella-Gutiérrez, J. M. Silla-Martínez, T. Gabaldón, trimAl: A tool for automated alignment trimming in large-scale phylogenetic analyses. *Bioinformatics* **25**, 1972–1973 (2009). doi:10.1093/bioinformatics/btp348 Medline
51. L.-T. Nguyen, H. A. Schmidt, A. von Haeseler, B. Q. Minh, IQ-TREE: A fast and effective stochastic algorithm for estimating maximum-likelihood phylogenies. *Mol. Biol. Evol.* **32**, 268–274 (2015). doi:10.1093/molbev/msu300 Medline
52. I. Letunic, P. Bork, Interactive Tree of Life (iTOL) v6: Recent updates to the phylogenetic tree display and annotation tool. *Nucleic Acids Res.* **52** (W1), W78–W82 (2024). doi:10.1093/nar/gkae268 Medline
53. L. J. Revell, phytools 2.0: An updated R ecosystem for phylogenetic comparative methods (and other things). *PeerJ* **12**, e16505 (2024). doi:10.7717/peerj.16505 Medline
54. G. E. Crooks, G. Hon, J.-M. Chandonia, S. E. Brenner, WebLogo: A sequence logo generator. *Genome Res.* **14**, 1188–1190 (2004). doi:10.1101/gr.849004 Medline
55. S. Picelli, A. K. Björklund, B. Reinius, S. Sagasser, G. Winberg, R. Sandberg, Tn5 transposase and tagmentation procedures for massively scaled sequencing projects. *Genome Res.* **24**, 2033–2040 (2014). doi:10.1101/gr.177881.114 Medline
56. M. Martin, Cutadapt removes adapter sequences from high-throughput sequencing reads. *EMBnet. J.* **17**, 10 (2011). doi:10.14806/ej.17.1.200
57. M. Vasimuddin, S. Misra, H. Li, S. Aluru, "Efficient architecture-aware acceleration of BWA-MEM for multicore systems," 2019 IEEE International Parallel and Distributed Processing Symposium (IPDPS), Rio de Janeiro, Brazil, 20 to 24 May 2019 (IEEE, 2019); https://ieeexplore.ieee.org/document/8820962/.
58. P. Danecek, J. K. Bonfield, J. Liddle, J. Marshall, V. Ohan, M. O. Pollard, A. Whitwham, T. Keane, S. A. McCarthy, R. M. Davies, H. Li, Twelve years of SAMtools and BCFtools. *Gigascience* **10**, giab008 (2021). doi:10.1093/gigascience/giab008 Medline
59. T. L. Bailey, M. Boden, F. A. Buske, M. Frith, C. E. Grant, L. Clementi, J. Ren, W. W. Li, W. S. Noble, MEME SUITE: Tools for motif discovery and searching. *Nucleic Acids Res.* **37**, W202–W208 (2009). doi:10.1093/nar/gkp335 Medline
60. T. J. Wheeler, S. R. Eddy, nhmmer: DNA homology search with profile HMMs.

Bioinformatics **29**, 2487–2489 (2013). doi:10.1093/bioinformatics/btt403 Medline
61. E. P. Nawrocki, S. R. Eddy, Infernal 1.1: 100-fold faster RNA homology searches. *Bioinformatics* **29**, 2933–2935 (2013). doi:10.1093/bioinformatics/btt509 Medline
62. E. Rivas, J. Clements, S. R. Eddy, A statistical test for conserved RNA structure shows lack of evidence for structure in lncRNAs. *Nat. Methods* **14**, 45–48 (2017). doi:10.1038/nmeth.4066 Medline
63. C. E. Grant, T. L. Bailey, W. S. Noble, FIMO: Scanning for occurrences of a given motif. *Bioinformatics* **27**, 1017–1018 (2011). doi:10.1093/bioinformatics/btr064 Medline
64. A. Punjani, J. L. Rubinstein, D. J. Fleet, M. A. Brubaker, cryoSPARC: Algorithms for rapid unsupervised cryo-EM structure determination. *Nat. Methods* **14**, 290–296 (2017). doi:10.1038/nmeth.4169 Medline
65. T. Bepler, A. Morin, M. Rapp, J. Brasch, L. Shapiro, A. J. Noble, B. Berger, Positive-unlabeled convolutional neural networks for particle picking in cryo-electron micrographs. *Nat. Methods* **16**, 1153–1160 (2019). doi:10.1038/s41592-019-0575-8 Medline
66. R. W. Grosse-Kunstleve, N. K. Sauter, N. W. Moriarty, P. D. Adams, The*Computational Crystallography Toolbox*: Crystallographic algorithms in a reusable software framework. *J. Appl. Cryst.* **35**, 126–136 (2002). doi:10.1107/S0021889801017824
67. K. Jamali, L. Käll, R. Zhang, A. Brown, D. Kimanius, S. H. W. Scheres, Automated model building and protein identification in cryo-EM maps. *Nature* **628**, 450–457 (2024). doi:10.1038/s41586-024-07215-4 Medline
68. P. Emsley, K. Cowtan, Coot: Model-building tools for molecular graphics. *Acta Crystallogr. D Biol. Crystallogr.* **60**, 2126–2132 (2004). doi:10.1107/S0907444904019158 Medline
69. P. D. Adams, P. V. Afonine, G. Bunkóczi, V. B. Chen, I. W. Davis, N. Echols, J. J. Headd, L.-W. Hung, G. J. Kapral, R. W. Grosse-Kunstleve, A. J. McCoy, N. W. Moriarty, R. Oeffner, R. J. Read, D. C. Richardson, J. S. Richardson, T. C. Terwilliger, P. H. Zwart, PHENIX: A comprehensive Python-based system for macromolecular structure solution. *Acta Crystallogr. D Biol. Crystallogr.* **66**, 213–221 (2010). doi:10.1107/S0907444909052925 Medline
70. S. Srikant, C. K. Guegler, M. T. Laub, The evolution of a counter-defense mechanism in a virus constrains its host range. *eLife* **11**, e79549 (2022). doi:10.7554/eLife.79549 Medline
71. D. E. Deatherage, J. E. Barrick, Identification of mutations in laboratory-evolved microbes from next-generation sequencing data using breseq. *Methods Mol. Biol.* **1151**, 165–188 (2014). doi:10.1007/978-1-4939-0554-6_12 Medline
72. R. Odegrip, A. S. Nilsson, E. Haggård-Ljungquist, Identification of a gene encoding a functional reverse transcriptase within a highly variable locus in the P2-like coliphages. *J. Bacteriol.* **188**, 1643–1647 (2006). doi:10.1128/JB.188.4.1643-1647.2006 Medline
73. C. Hill, L. A. Miller, T. R. Klaenhammer, Nucleotide sequence and distribution of the pTR2030 resistance determinant (hsp) which aborts bacteriophage infection in lactococci. *Appl. Environ. Microbiol.* **56**, 2255–2258 (1990). doi:10.1128/aem.56.7.2255-2258.1990 Medline
74. P. K. Dinsmore, T. R. Klaenhammer, Phenotypic Consequences of Altering the Copy Number of abiA, a Gene Responsible for Aborting Bacteriophage Infections in Lactococcus lactis. *Appl. Environ. Microbiol.* **60**, 1129–1136 (1994). doi:10.1128/aem.60.4.1129-1136.1994 Medline

ACKNOWLEDGMENTS

We thank B. Singal, D. F. Martinez, and W. Arnold at Stanford cEMc for assistance with data collection and pixel size recalibration; J. Wang, F. Yang, K. Xu, and S. Zhang for their help with cryo-EM computational analysis and model refinement; V. Wu, A. Kladwang, G. Kim, J. M. Lee, and B. Johnson for the technical assistance; J. Shin and R. Kretsch for helpful discussions; and the entire Gao lab for their support and advice. **Funding**: C.A. is supported by a training grant from NIH Cellular and Molecular Training Grant (NIGMS, grant no. 5T32GM007276). A.G. is supported by the G. Harold and Leila Y. Mathers Foundation (grant no. MF-2303-04116), the Esther Ehrman Lazard Faculty Scholars Program, and Stanford Bio-X. **Author contributions**: H.L. and A.G. conducted bioinformatics analyses. H.L. and C.A. performed phage plaque assays and sequencing experiments. P.D. and C.A. purified proteins and performed biochemical experiments. P.D. prepared cryo-EM samples. P.D. and H.W. determined cryo-EM structures, including data acquisition, computational processing, and atomic model building. P.D. and H.L. analyzed the structures and prepared figures. H.L. isolated and characterized escape phages. A.G. supervised research. P.D., H.L., and A.G. wrote the manuscript. **Competing interests:** The authors declare that they have no competing interests. **Data, code, and materials availability**: Expression plasmids for DRT3 systems have been deposited in Addgene (#255316 and #255317). The cryo-EM density maps and atomic models generated in this study have been deposited in the Electron Microscopy Data Bank (EMDB) and the Protein Data Bank (PDB), respectively. The EMDB accession numbers for the cryo-EM maps are as follows: EMD-76001 (elongating composite map), EMD-73864 (elongating hexamer), EMD-75821 (elongating protomer), EMD-75826 (elongating EcDrt3a-ncRNA), EMD-76002 (resting composite map), EMD-73865 (resting hexamer), EMD-75828 (resting protomer), EMD-75830 (resting EcDrt3a-ncRNA), EMD-75981 (hexamer, ddATP+dCTP), EMD-75982 (protomer, ddATP+dCTP), and EMD-75983 (EcDrt3a-ncRNA, ddATP+dCTP). The atomic models for the elongating and resting state hexamers have been deposited in the PDB under accession codes 9Z6Y and 9Z6Z, respectively.

SUPPLEMENTARY MATERIALS

science.sciencemag.org/cgi/content/full/science.aeb1656/DC1
Materials and Methods
Figs. S1 to S14
Table S1
References (*47*–*74*)
MDAR Reproducibility Checklist
Data S1 to S8

Submitted 21 November 2025; accepted 08 April 2026
Published online 16 April 2026
10.1126/science.aeb1656

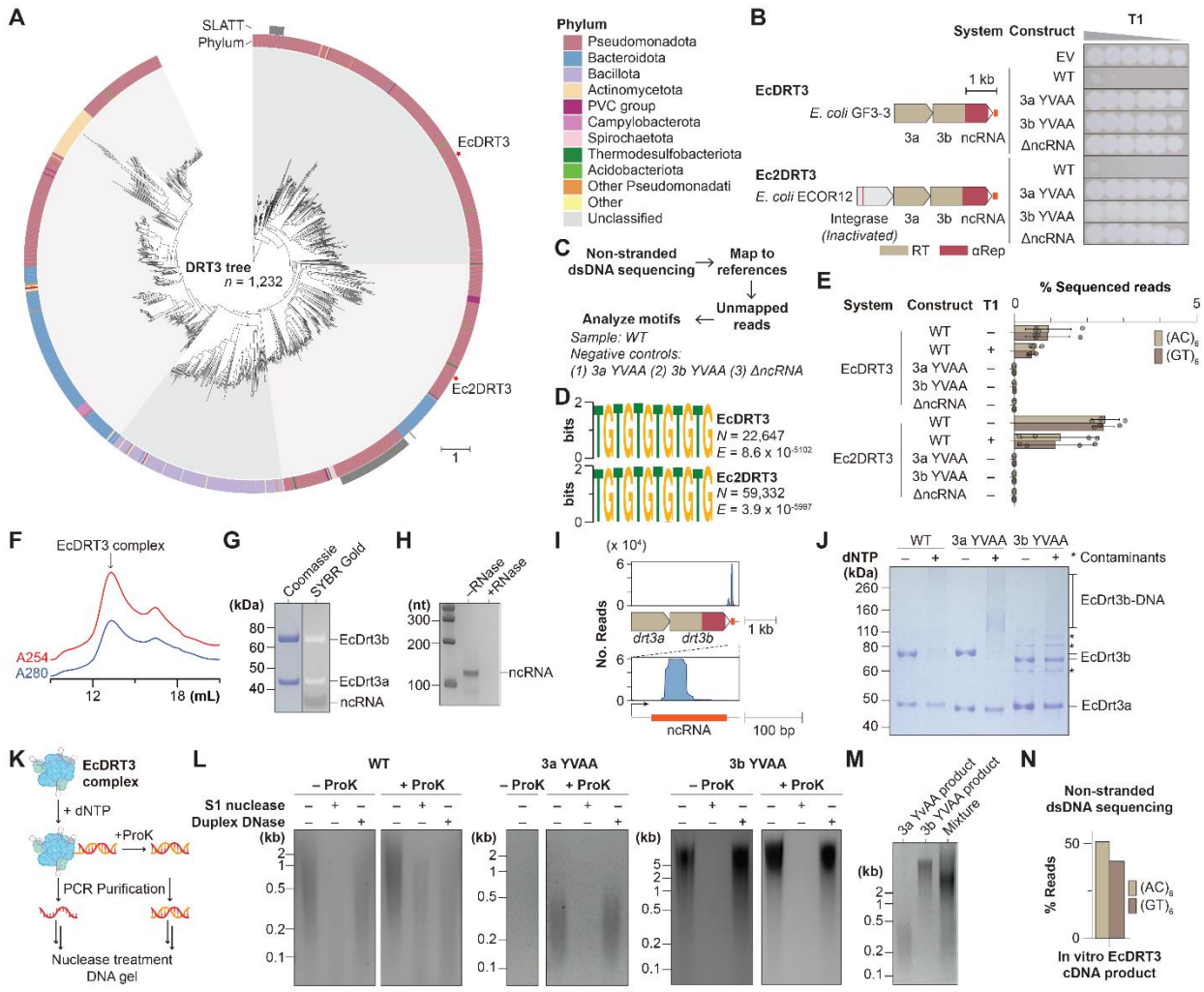

Fig. 1. Fig. 1. DRT3 forms an RNP complex that constitutively synthesizes repetitive alternating poly(GT:AC) double-stranded DNA. (**A**) Phylogenetic tree of the DRT3 system (*n* = 1,232 representatives) based on a concatenated alignment of the Drt3a and Drt3b proteins. Two minor clades (83 representatives; 7%) are associated with an additional SLATT-domain membrane protein (*46*), extending previous observations (*20*). (**B**) Anti-phage activity of two DRT3 systems from distinct clades against *Escherichia* phage T1. Catalytic mutants (YVAA) denote the following alanine substitutions: EcDRT3a (D197A/D198A), EcDRT3b (D291A/D292A), Ec2DRT3a (D197A/D198A), and Ec2DRT3b (D278A/D279A). (**C**) Analysis of non-stranded dsDNA sequencing of DRT3-expressing cells. (**D**) Sequence logos of motifs identified from the unmapped read fraction of the wildtype DRT3 systems. (**E**) Percentage of sequencing reads containing an $(AC)_6$ or $(GT)_6$ motif across different conditions (4 replicates each). (**F** and **G**) Size-exclusion chromatogram (F) and SDS-PAGE analysis (G) of the purified EcDRT3 complex. (**H**) Urea-PAGE analysis of nucleic acids co-purified with EcDRT3. (**I**) RNA sequencing reads for the EcDRT3 ncRNA mapped to the EcDRT3 locus. (**J**) SDS-PAGE analysis of the wildtype EcDRT3 complex or active site mutants (3a YVAA and 3b YVAA) after incubation with dNTPs. (**K** and **L**) Sample preparation workflow (K) and DNA agarose gel analysis (L) of the cDNA products. (**M**) DNA agarose gel analysis of the EcDRT3 3a YVAA and 3b YVAA products individually and as a mixture. (**N**) Quantification of poly(GT) and poly(AC) reads for the EcDRT3 cDNA product. WT, wild type.

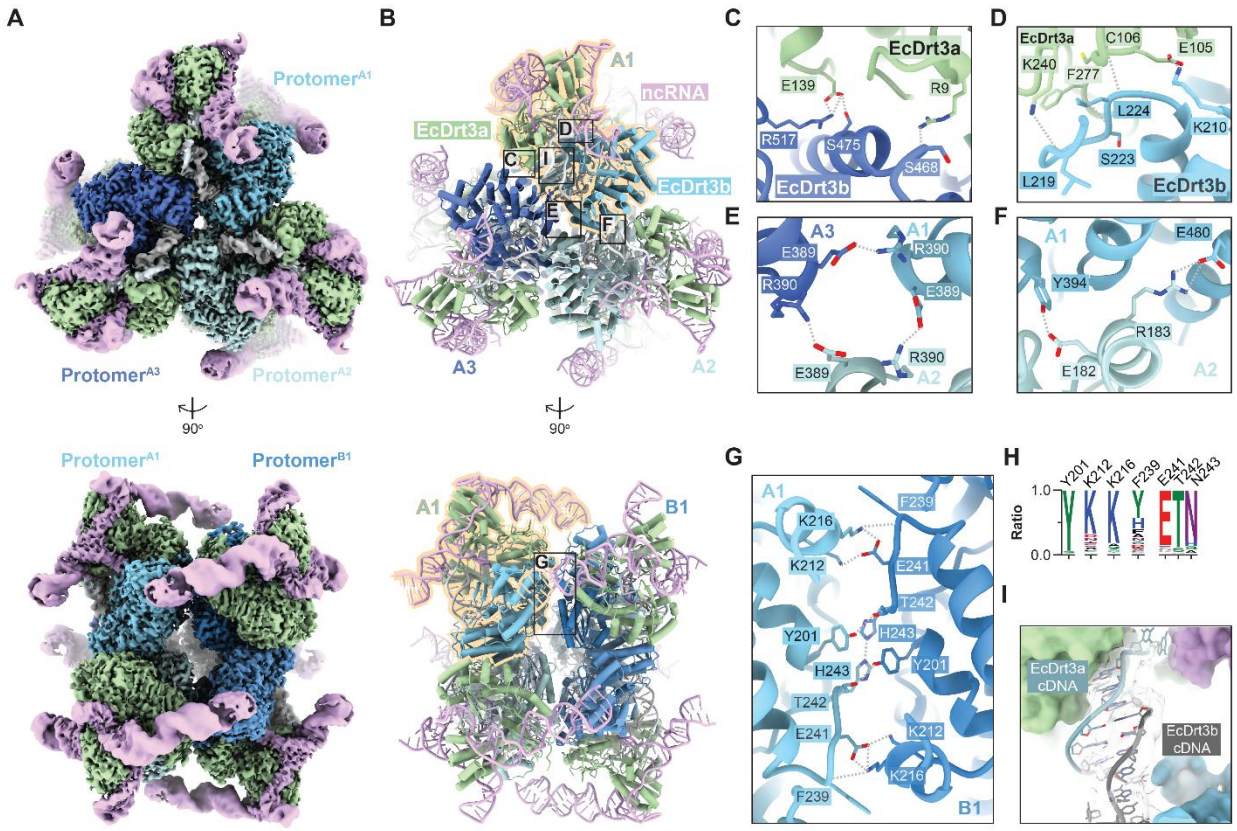

Fig. 2. Cryo-EM structure of the elongating EcDRT3 hexamer. (**A** and **B**) Composite cryo-EM maps (A) and atomic models (B) for the EcDRT3 complex in the presence of dNTPs. A single protomer is outlined in yellow. (**C** to **F**) Intra-subunit interactions between EcDrt3a and adjacent EcDrt3b subunits [(C) and (D)] or between two EcDrt3b subunits [(E) and (F)] within an EcDRT3 trimer layer. (**G**) Interactions between two EcDrt3b subunits from opposing trimer layers. (**H**) Sequence logos for residues in (G) from a multiple sequence alignment of EcDrt3b homologs. (**I**) EcDRT3 product DNA duplex.

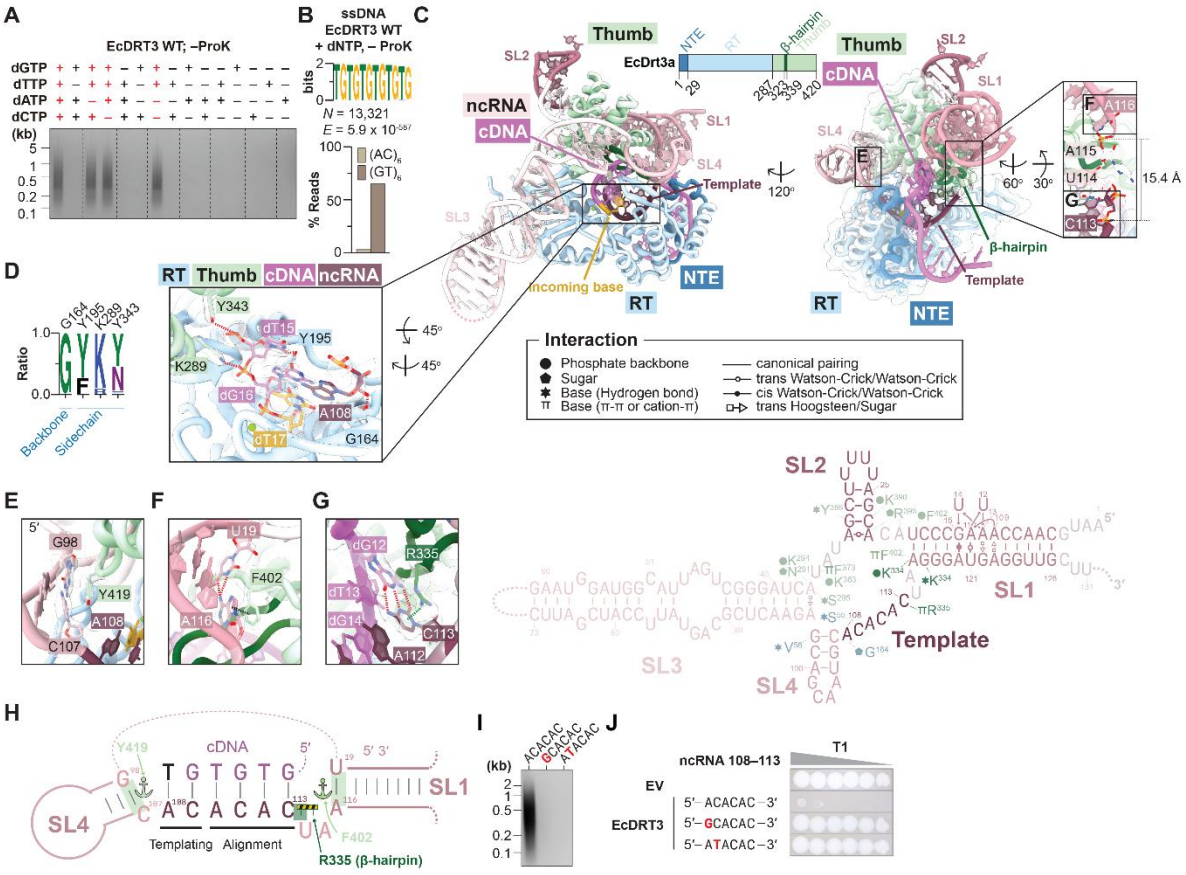

Fig. 3. EcDrt3a synthesizes poly(GT) ssDNA using the ACACAC motif of the ncRNA as a template. (**A**) DNA agarose gel analysis of the EcDrt3a product in the presence of distinct dNTP combinations. (**B**) Sequence logo of the motif identified from the in vitro EcDrt3a cDNA product, along with quantification of poly(GT) and poly(AC) reads. (**C**) Overall structure of the elongating EcDrt3a-ncRNA complex (top) and the secondary structure diagram of the ncRNA (bottom). NTE, N-terminal extension. (**D** to **G**) Interactions between EcDrt3a and ncRNA. Cryo-EM maps are shown as surfaces. (**H**) Summary of molecular interactions that position the ncRNA ACACAC motif. (**I**) Agarose gel electrophoresis of DNA products synthesized by EcDRT3 with mutant ncRNAs. (**J**) Anti-phage activity of EcDRT3 ncRNA mutants against phage T1.

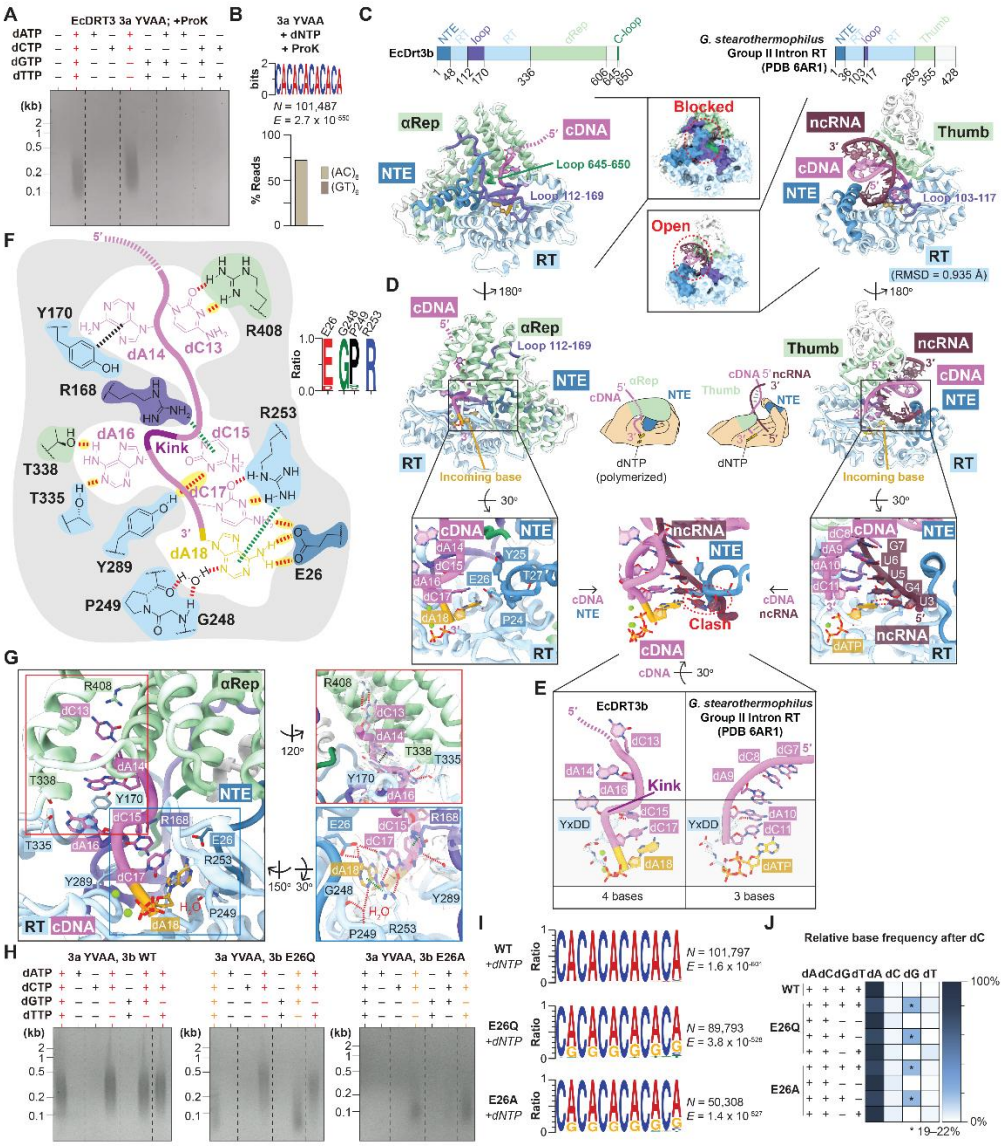

Fig. 4. EcDrt3b synthesizes poly(AC) ssDNA without a nucleic acid template. (**A**) DNA agarose gel analysis of the EcDrt3b products synthesized by the EcDRT3 3a YVAA complex in vitro. (**B**) Sequence logo of the motif identified from the in vitro EcDrt3b cDNA product, along with quantification of poly(GT) and poly(AC) reads. (**C** to **E**) Comparative structural analysis of the putative ncRNA entry region (C), template RNA position (D), and the conformation of the cDNA product in the active site (E) between EcDrt3b and the *G. stearothermophilus* group II intron reverse transcriptase (PDB: 6AR1) (*30*). Proteins are shown as surfaces in the inset of (C) to highlight the blockage of the path for the putative template RNA by both the C terminus (residues 645–650) and the extended loop (residues 112–169) in EcDrt3b, whereas the corresponding region is open in group II intron RT. EcDrt3b NTE and the template RNA of *G. stearothermophilus* group II intron is overlaid in panel D to show the steric clash at the templating base. (**F** and **G**) Summary of the interactions between EcDrt3b and the last six bases at the 3′ end of its cDNA product (F) and the corresponding structural views (G). Hydrogen bonds, π-π interactions, and cation-π interactions are shown in red, black, and green dotted lines, respectively. Base-specific interactions are highlighted in yellow. (**H**) Agarose gel of in vitro DNA products synthesized by the EcDRT3 3a-YVAA/3b-WT, 3a-YVAA/3b-E26Q, and 3a-YVAA/3b-E26A complexes. (**I**) Sequence logos of cDNA motifs generated by these variants in the presence of all four dNTPs. (**J**) Relative base incorporation frequencies following dC in the cDNA products.

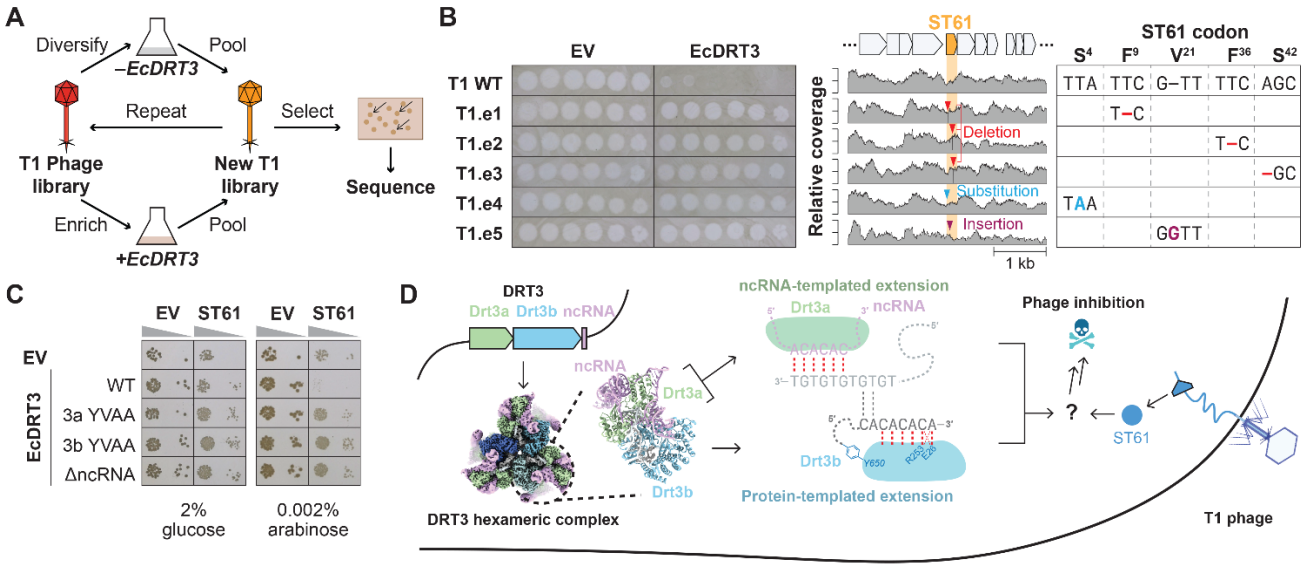

Fig. 5. EcDRT3-mediated defense against phage T1 requires protein ST61. (**A**) A schematic for the isolation of escaper phages against EcDRT3. (**B**) Features of the isolated escaper phages. (Left) Plaque assays of *E. coli* cells with empty vector (EV) or EcDRT3 against T1 wildtype or escapers 1–5. (Middle) Coverage tracks from whole genome sequencing of phages at the selected genomic loci. (Right) Mutations observed in the ST61 open reading frame. (**C**) *E. coli* co-transformation assay with the EcDRT3 complex and T1 ST61. (**D**) Proposed molecular mechanism of EcDRT3-mediated antiphage immunity.

Protein-templated synthesis of dinucleotide repeat DNA by an antiphage reverse transcriptase

Pujuan Deng, Hyunbin Lee, Carlo Armijo, Haoqing Wang, and Alex Gao

*Science***Ahead of Print** DOI: 10.1126/science.aed1656